

# Role of Water Molecule in Enhancing the Proton Conductivity on Graphene Oxide Film at High Humidity Condition

Gum-Chol Ri, Jin-Song Kim, and Chol-Jun Yu\*

*Department of Computational Materials Design (CMD),*

*Faculty of Materials Science, Kim Il Sung University,*

*Ryongnam-Dong, Taesong District, Pyongyang,*

*Democratic People's Republic of Korea*

(Dated: November 27, 2018)

## Abstract

Reduced graphene oxide (rGO) films can be utilized as a solid proton conductor due to their good in-plane proton conductivity under humid condition. We devise the series of water-adsorbed monolayer and bilayer rGO models as increasing the oxidation degree and water content. By using first-principles method, we predict the migration paths and kinetic activation barriers for the in-plane proton transports on these rGO films. We suggest two different mechanisms of epoxy- and water-mediated proton transports, and conclude that the water-mediated transport is really occurred due to much lower activation energy ( $\sim 0.16$  eV) than that of the epoxy-mediated one and being close to the experimental value.

---

\* E-mail: ryongnam14@yahoo.com

## I. INTRODUCTION

Reduced graphene oxide (rGO) films with a controlled reduction degree have been reported to possess a good in-plane proton conductivity at room temperature and high relative humidity (RH) condition [1–7]. Therefore, rGO films can be a promising solid proton conductor, which is of great importance in electrochemical energy generating and selective material sieving systems. It was already known that proton can pass across monolayer graphene [8–11] or few layer GO sheet [12–14], but only through atomic-scale defects created on those nanosheets. If no defect, graphene and GO sheet are factually impermeable to proton under ambient condition due to a dense, delocalized electronic cloud formed by graphene’s  $\pi$ -orbitals [15, 16]. In fact, Hu *et al.* [8] measured through-plane proton conductivity of monolayer graphene sheet as  $\sigma \approx 2\sim 4$  mS/cm<sup>2</sup> at room temperature, and obtained the activation barrier as  $E_a \approx 0.78$  eV, for which first-principles calculations yield even higher values of 1.2~2.2 eV [17, 18]. Decorating graphene with catalytic metal nanoparticles like Pt reduces the activation energy by  $\sim 0.65$  eV [8], which is still relatively high. Therefore, research effort has been focused on the in-plane proton transport on the sheet. However, the kinetic activation barrier for proton or hydrogen atom diffusion on the graphene sheet was turned out to be high as well, like 0.9 eV due to a strong binding of H to graphene sheet, while it reduces by 0.42 eV when mediated by water molecules [19].

Unlike graphene, GO sheet has oxygenated functional groups such as epoxy (–O–) and hydroxy (–OH) groups, which form one-dimensional hydrogen-bonded channels for proton transport [20–24]. According to the measurements by Hatakeyama *et al.* [2, 4–6], the in-plane proton conductivity of rGO film is  $\sim 2.4$  mS/cm ( $E_a = 0.12$  eV) at 278 K and 90% RH. When added some functional groups to GO, forming e.g. GO-Nafion hybrid or sulfonated GO complexes, the proton conductivity was enhanced [1, 3, 25–27]. These experimental works imply that uptake and retention of water in the GO nanosheet are a key factor for high proton conductivity. It was expected that the hydrophilic functional groups such as epoxy groups in the GO nanosheet can readily adsorb water and support the formation of channels for proton stream on the sheet. In spite of several experimental reports, no theoretical work to illustrate the mechanism of enhancing proton transport by water adhesion to GO sheet has been reported.

In this work we investigate the atomistic structures of water-adsorbed GO sheets and

in-plane proton migrations by first-principles method [38]. We use pseudopotential plane wave method within the density functional theory (DFT) framework, and minimum energy path method to calculate the activation barriers for the in-plane proton migrations together with bond valence sum (BVS) analysis for prediction of adsorbing sites of proton. Dispersive interactions between the sheets and molecules are included using the flavour of vdW-DF-OB86 [28].

## II. COMPUTATIONAL METHODS

All calculations in this work are performed with the pseudopotential plane-wave method as implemented in Quantum ESPRESSO package (version 5.3) [29]. The ultrasoft pseudopotentials are used to describe ion-electron interaction [39]. The Perdew-Burke-Ernzerhof (PBE) functional [30] within generalized gradient approximation (GGA) is used for exchange-correlation interaction between valence electrons. In addition, for van der Waals (vdW) dispersive interaction between graphene sheets and possibly between water molecules and graphene sheet, the vdW energy provided by vdW-DF-OB86 method [28] is added to the DFT total energy. As the major computational parameters, the plane-wave cutoff energies are set to be 40 Ry for wave function and 400 Ry for electron density, and the Monkhorst-Pack special  $k$ -points are set to be  $(2 \times 2 \times 5)$  for bilayer sheet and  $(2 \times 2 \times 1)$  for monolayer sheet, providing an accuracy of 5 meV per carbon atom for total energy. Self-consistent convergence threshold for total energy is  $10^{-9}$  Ry, and the convergence threshold for atomic force in structural relaxations is  $8 \times 10^{-4}$  Ry/Bohr. Methfessel-Paxton first-order spreading with the gaussian spreading factor of 0.2 Ry is applied to the Brillouin-zone integration.

We calculate the oxygen binding energy as a function of the number of oxygen atoms in reduced graphene oxide (rGO) and compared with the previous first-principles calculations [20] in order to check the validity of the computational parameters and our rGO supercell models. The binding energy  $E_b$  can be calculated as follows,

$$E_b = \frac{1}{N_O}(E_{\text{rGO}} - E_G - N_O E_O) \quad (1)$$

where  $E_{\text{rGO}}$ ,  $E_G$  and  $E_O$  are the total energies of rGO, graphene and oxygen-involved supercells, and  $N_O$  is the number of oxygen atoms involved in the rGO model. Similarly, water

binding energy per molecule can be calculated as follows,

$$E_b = \frac{1}{N_{\text{H}_2\text{O}}}(E_{\text{hyd-rGO}} - E_{\text{rGO}} - N_{\text{H}_2\text{O}}E_{\text{H}_2\text{O}}) \quad (2)$$

where  $E_{\text{hyd-rGO}}$  and  $E_{\text{H}_2\text{O}}$  are the total energies of water-adsorbed rGO supercell and H<sub>2</sub>O-involved supercell, respectively, and  $N_{\text{H}_2\text{O}}$  is the number of water molecules. Meanwhile, proton adsorption energy into water-adsorbed rGO sheet is calculated as follows,

$$E_{\text{ad}} = E_{\text{p-hyd-rGO}} - E_{\text{hyd-rGO}} - \frac{1}{2}E_{\text{H}_2} \quad (3)$$

where  $E_{\text{p-hyd-rGO}}$  and  $E_{\text{H}_2}$  are the total energies of proton-adsorbed hydrous rGO and H<sub>2</sub>-involved supercells.

To predict the possible positions of inserted H<sup>+</sup> ion into the water-adsorbed rGO sheets, bond valence sum (BVS) method [31] is applied, where BVS at the  $\mathbf{r}$  position,  $B(\mathbf{r})$ , can be calculated as follows,

$$B(\mathbf{r}) = \sum_i \exp \left[ \frac{R_0 - R_i(\mathbf{r})}{b} \right] \quad (4)$$

Here,  $R_i(\mathbf{r}) = |\mathbf{r} - \mathbf{R}_i|$  ( $\mathbf{R}_i$  for oxygen positions),  $b$  ( $= 0.37 \text{ \AA}$ ) is a constant, and  $R_0$  is a constant specific to the pair of hydrogen and oxygen atoms, which can be calculated based on atomic size ( $r$ ) and electronegativity ( $c$ ) parameters as follows [32],

$$R_0 = r_{\text{H}} + r_{\text{O}} - \frac{r_{\text{H}}r_{\text{O}}(\sqrt{c_{\text{H}}} - \sqrt{c_{\text{O}}})^2}{c_{\text{H}}r_{\text{H}} + c_{\text{O}}r_{\text{O}}} \quad (5)$$

where  $r_{\text{H}} = 0.38 \text{ \AA}$ ,  $r_{\text{O}} = 0.63 \text{ \AA}$ ,  $c_{\text{H}} = 0.89$ , and  $c_{\text{O}} = 3.15$  [33]. The values of  $B(\mathbf{r})$  at the positions of hydrogen atoms are evaluated to be almost 3 and the difference of  $B(\mathbf{r})$  from this value are calculated for the whole space with a grid resolution of  $0.1 \text{ \AA}$ .

To calculate the migration barriers for the in-plane proton transport, we apply the climbing image nudged elastic band (NEB) method [34]. The supercell dimensions are fixed at the optimized supercell size during the NEB runs, while all the atoms are relaxed with the convergence criteria for the forces of  $0.05 \text{ eV/\AA}$ . The number of images adopted in this work are tuned so that the distance between neighbouring NEB images can be  $\sim 1 \text{ \AA}$ .

### III. RESULTS AND DISCUSSION

We first make the atomistic modelling of rGO sheets and build their supercells. For the types of rGO sheet, we consider monolayer and bilayer sheets with different oxidation degree

(*i.e.*, reduction degree) measured by the ratio  $O/(C+O)$  [2], which is changed from 14.3% to 33.3% in this study. The orthogonal  $(7 \times 3)$  and  $(4 \times 2)$  cells are employed for the basal plane of graphene sheet, which contain the carbon atoms of 72 and 32 respectively. When making the modelling of rGO sheets, the same number of oxygen atoms are adsorbed on both sides of graphene sheet to form epoxy groups, which are arranged as a row to form a path for the in-plane proton migration, based on the established fact that the epoxy groups are clustered on the rGO sheet [20]. Then, the numbers of oxygen atoms can be 12 for the case of  $(7 \times 3)$  cell and 8, 12, 16 for the case of  $(4 \times 2)$  cell, which correspond to chemical formula of  $C_{72}O_{12}$  ( $O/(C+O) = 14.3\%$ ),  $C_{32}O_8$  (20.0%),  $C_{32}O_{12}$  (27.3%) and  $C_{32}O_{16}$  (33.3%). The simulated lattice constant of 0.246 nm and the vacuum layer of 1.5 nm were used throughout the work.

We checked the oxygen binding energy per atom after atomic relaxations of monolayer rGO sheets with  $(7 \times 3)$  cells. The calculated oxygen binding energy as a function of oxygen number was confirmed to be agreed well with the previous results [20]. The calculated O binding energy is shown in Fig. 1. In the case of  $C_{72}O_{12}$  system the value of 2.64 eV in this work is reasonably agreed with the previous value of 2.90 eV [20]. We make an interpolation curve using the calculated values at  $n = 1, 2, 3, 4, 12, 16,$  and  $20$ , resulting in the function of  $E_b(n) = 2.833 - 0.763/\sqrt{n}$  (eV). When compared with the previous theoretical result [20], our values are slightly underestimated possibly due to the inclusion of vdW energy in this

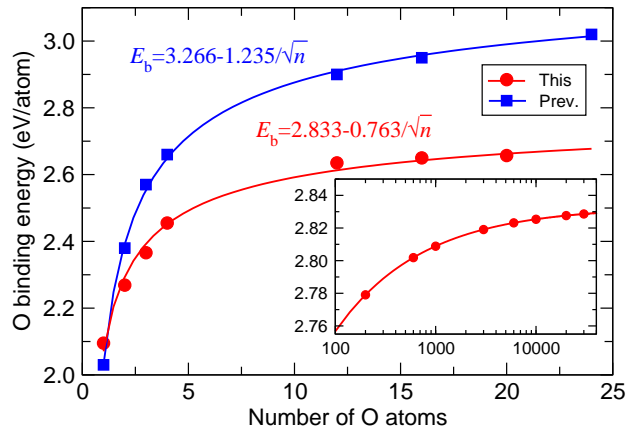


FIG. 1: Oxygen binding energy as increasing the number of oxygen atoms in reduced graphene oxide. Inset shows an extension to over 100 oxygen atoms using the interpolation curve. Blue line shows the previous theoretical result [20].

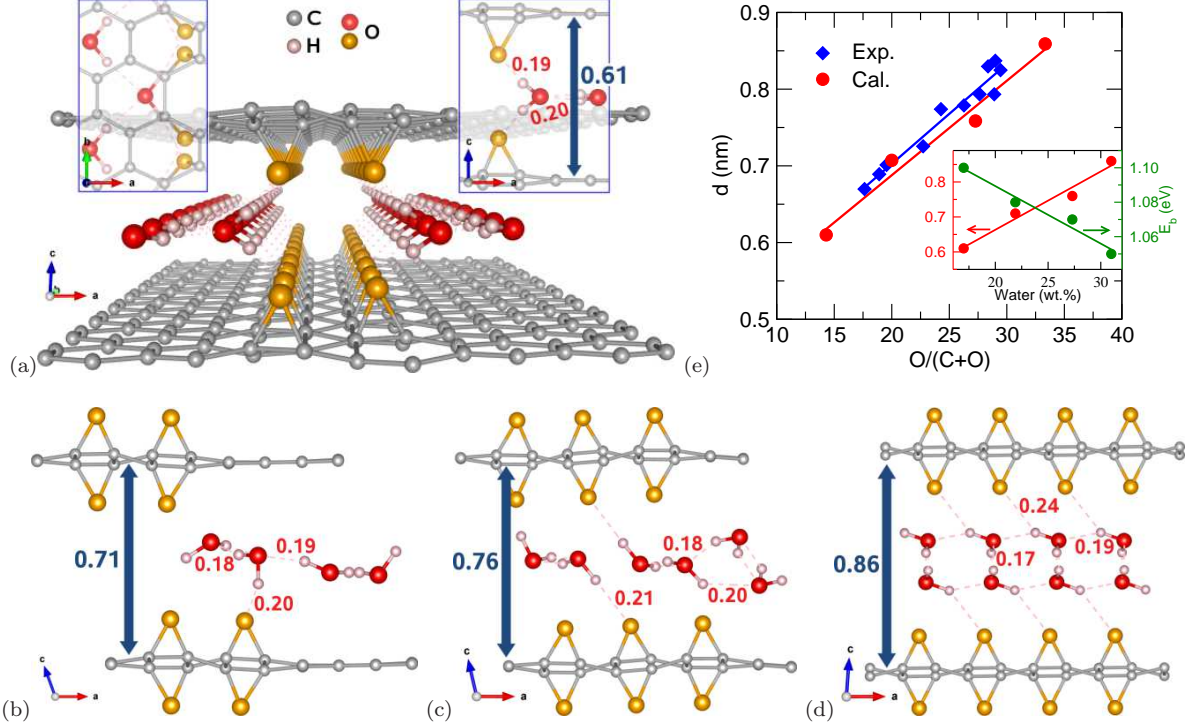


FIG. 2: Optimized atomistic structures of water-intercalated bilayer rGO with chemical formula of (a)  $C_{72}O_{12} \cdot 12(H_2O)$  in perspective (centre), top (left) and side (right) views, (b)  $C_{32}O_8 \cdot 8(H_2O)$ , (c)  $C_{32}O_{12} \cdot 12(H_2O)$ , and (d)  $C_{32}O_{16} \cdot 16(H_2O)$  in side view. Interlayer distance and hydrogen bond length (pink dashed line) in the unit of nm are shown. (e) Interlayer distance  $d$  as a function of oxidation degree ( $O/(C+O)$ (%)), where Exp. means the experimental values in Ref. [2] and Cal. the calculated values in this work. Inset shows the interlayer distance and water binding energy per molecule ( $E_b$ ) as functions of water content (wt.%).

work.

Then water molecules are adsorbed on the monolayer rGO sheet or intercalated into interlayer space between the bilayer rGO sheets. As shown in Fig. 2, the adsorbed water molecules are anchored to the epoxy groups on rGO sheet, while the intercalated water molecules are placed on the centre of carbon hexagon of the graphene sheet. Here, different water contents are considered by tuning the number of water molecules, producing monolayer  $C_{72}O_{12} \cdot 6(H_2O)$  (water content = 9.3 wt%) and bilayer  $C_{72}O_{12} \cdot 12(H_2O)$  (17.0%),  $C_{32}O_8 \cdot 8(H_2O)$  (21.9%),  $C_{32}O_{12} \cdot 12(H_2O)$  (27.3%) and  $C_{32}O_{16} \cdot 16(H_2O)$  (31.0%). The water contents of 21 and 31% correspond to  $\sim 30$  and 90% RH in the GO paper from the previous

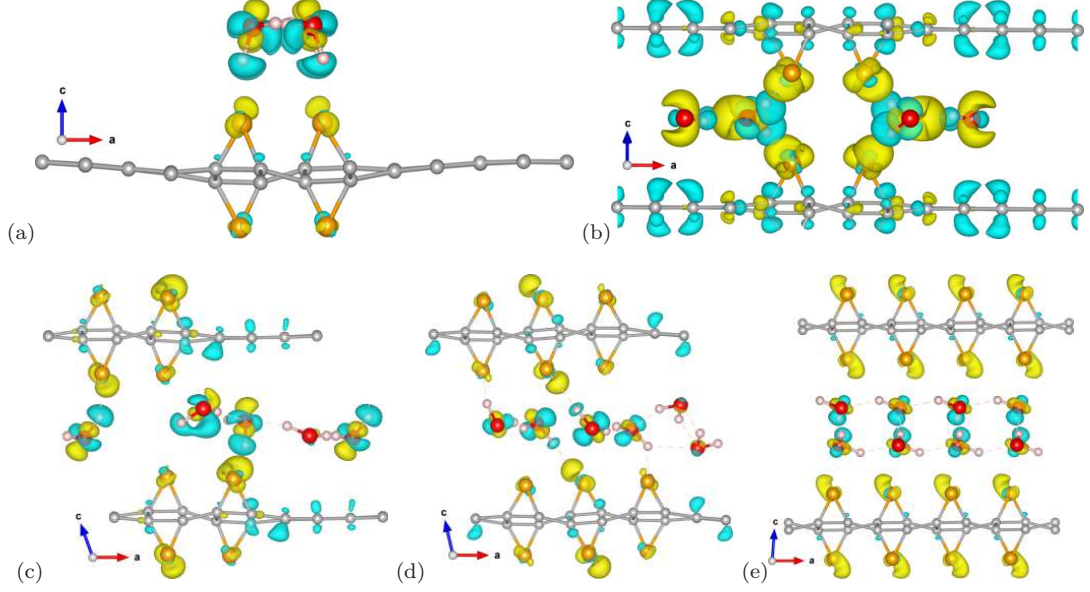


FIG. 3: Isosurface plot of electronic charge density difference between water-adsorbed or water-intercalated rGO and pristine rGO at the value of  $0.002 |e|/\text{\AA}^3$ . Yellow (cyan) color represents the charge accumulation (depletion). Small balls of grey, pink, red and brown colors represent the carbon, hydrogen, oxygen atoms of epoxy group and water molecule, respectively.

experimental works [4, 35, 36].

The structural optimizations of these water-intercalated bilayer rGO supercells were per-

TABLE I: Overview of rGO and the series of water-adsorbed rGO models with oxidation degree ( $O/(C+O)$ ) and water content in weight percentage. Given are the interlayer distance ( $d$ ) and the activation energy ( $E_a$ ).

Model	Layer type	O/(C+O) (%)	Water (wt.%)	$d$ (nm)	$E_a$ (eV)
$C_{72}O_{12}$	mono	14.3	—	—	0.35
$C_{72}O_{12} \cdot 6(H_2O)$	mono	14.3	9.3	—	0.16
$C_{72}O_{12} \cdot 12(H_2O)$	bi	14.3	17.0	0.61	0.17
$C_{32}O_8 \cdot 8(H_2O)$	bi	20.0	21.9	0.71	-
$C_{32}O_{12} \cdot 12(H_2O)$	bi	27.3	27.3	0.76	-
$C_{32}O_{16} \cdot 16(H_2O)$	bi	33.3	31.0	0.86	0.23

formed allowing atoms to be relaxed, while only atomic relaxations for the monolayer supercells. We found that for the bilayer models the interlayer distance increases as a linear function of oxidation degree, being agreed well with those of the rGO films prepared via photoreduction process in experiment [2] (Fig. 2(e)). Such linear increasing tendency of interlayer distance was also found when increasing the water content, as shown in the inset of Fig. 2(e) and Table I. This result is obvious given that the epoxide oxygen atoms attract the water molecules through hydrogen bond and thus more oxygen atoms can bind more intercalated water molecules, resulting in the expansion of interlayer space. Figures 2(a)–2(d) show the hydrogen bond lengths between the water molecules, which are of zigzag-type on the plane parallel to the basal graphene sheet, and between the epoxide oxygen atom and the water molecule. It can be seen that, while the hydrogen bond lengths between the water molecules are more or less invariable at the mean value of 0.19 nm, those with the epoxide oxygen atoms increase gradually from 0.19 nm at the oxidation degree of 14.3% to 0.20, 0.21, 0.24 nm at the oxidation degrees of 20.0, 27.3, 33.3%. It should be noted that those in the monolayer  $C_{72}O_{12}\cdot 6(H_2O)$  sheet are 0.17 and 0.23 nm for the former and the later hydrogen bonds. In order to estimate the strength of hydrogen bond, we calculated the water binding energy per molecule, which exhibits linearly decreasing tendency as increasing the water content (see the inset in Fig. 2(e)). This result coincides with that the hydrogen bond length between the epoxide oxygen atom and the intercalated water molecule increases gradually as increasing the water content, indicating a weakening of hydrogen bond at high humid condition. The electronic charge density difference also confirms that the charge transferring occurred upon water intercalation, where carbon and hydrogen atoms release while oxygen atoms gain electrons, become weakening when increasing water content, as shown in Fig. 3. In the case of monolayer  $C_{72}O_{12}\cdot 6(H_2O)$  model, the water binding energy was calculated to be 0.96 eV, being lower than those in the bilayer models. In addition, all the water binding energies were estimated to be negative, indicating that the water molecules are spontaneously bound to rGO films.

Using the determined structures of models, we proceeded with the in-plane proton transport on rGO film. As the preliminary check for the difficulty of the in-plane proton transport on the graphene sheet, we first considered the proton migration on the monolayer and bilayer graphene sheets. In these cases the proton can be adsorbed on the top of carbon atom with adsorption energies of  $-3.10$  eV (monolayer) and  $-13.87$  eV (bilayer), and migrates along

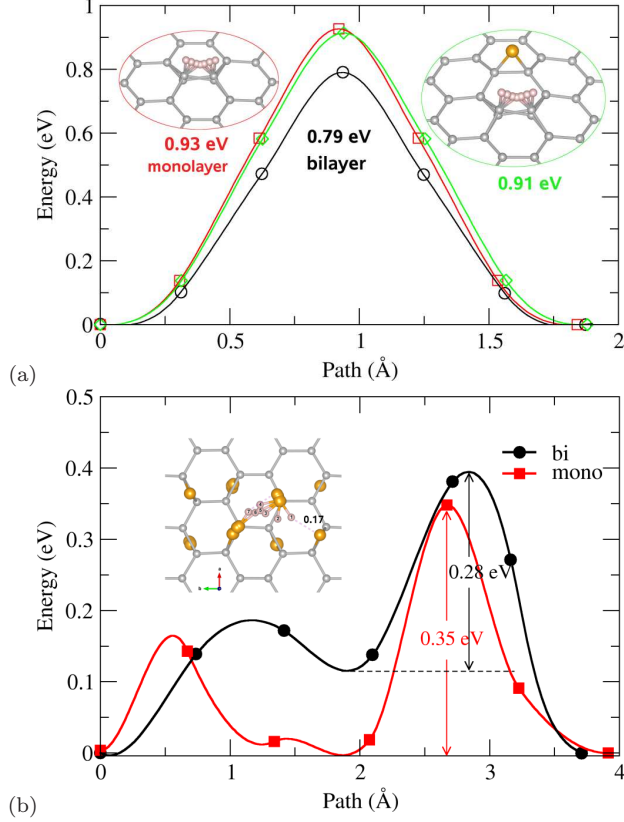


FIG. 4: Activation energy for proton migration (a) along the C–C bond in monolayer (red), bilayer (black) graphene and monolayer graphene with one epoxy group (green), and (b) along the one-dimensional hydrogen bonded channel formed by epoxy and hydroxy groups in monolayer (red) and bilayer (black)  $C_{72}O_{12}$  rGO model, where the inset shows the migration path with hydrogen bond length in the unit of nm for the case of bilayer rGO sheet.

the C–C bond with activation energies of 0.93 eV (monolayer), which is in good agreement with the previous result [19], and 0.79 eV (bilayer) (see Fig. 4(a)). The existence of an epoxy group around the migration path slightly reduces activation energy by 0.91 eV due to the hydrogen bonding interaction between the proton and the oxygen atom. We then considered the proton migration on the rGO sheet using  $C_{72}O_{12}$  model, where the proton was adsorbed on the top of the epoxide oxygen atom to become hydroxy group [37] (adsorption energies of  $-7.37$  and  $-14.47$  eV for the monolayer and bilayer sheets) and allowed to migrate to the neighbouring epoxide oxygen atom (*i.e.*  $-\text{OH} \rightarrow -\text{O}-$ ) with activation energies of 0.35 eV for the monolayer and 0.28 eV for the bilayer cases (see Fig. 4(b)). This confirms that the one-dimensional hydrogen-bonded channels formed by epoxy groups on the rGO sheet

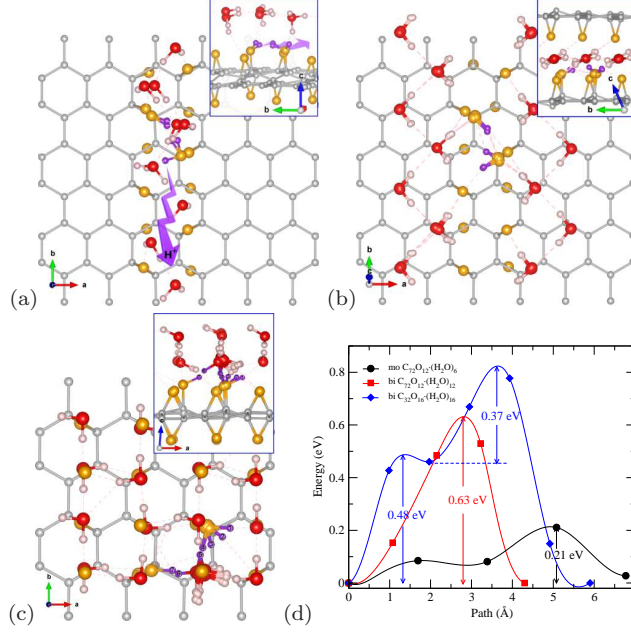


FIG. 5: Top view of migration paths for epoxy-mediated proton transport in (a) monolayer  $C_{72}O_{12}\cdot 6(H_2O)$ , (b) bilayer  $C_{72}O_{12}\cdot 12(H_2O)$  and (c) bilayer  $C_{32}O_{16}\cdot 16(H_2O)$  rGO films. Insets show the perspective view, and arrows indicate the proton migration. (d) Activation energies for these proton migrations.

can remarkably reduce activation energy for the in-plane proton transport [21–24]. In both cases of graphene and rGO sheets, bilayer films have lower activation energy than monolayer films, indicating that enhanced hydrogen-bonding interaction makes the proton transport fast.

For the cases of water-adsorbed or -intercalated rGO sheets, it is not easy to clarify the adsorption sites and migration paths of proton. Here we made a suggestion of two different migration mechanisms, namely, epoxy-mediated and water-mediated proton transports. In addition, mixing mechanism, *i.e.* epoxy-water-mediated proton transport, was not ruled out. In the former case we follow the same way as in the case of above mentioned rGO film, whereas in the latter case we performed  $\Delta BVS$  analysis to settle the adsorption sites of proton.

The activation barrier for the epoxy-mediated proton migration in the monolayer  $C_{72}O_{12}\cdot 6(H_2O)$  model was calculated to be 0.21 eV, which is lower than in its anhydrous counterpart  $C_{72}O_{12}$  model (0.35 eV) (Fig. 5). Such enhancement of proton migration is at-

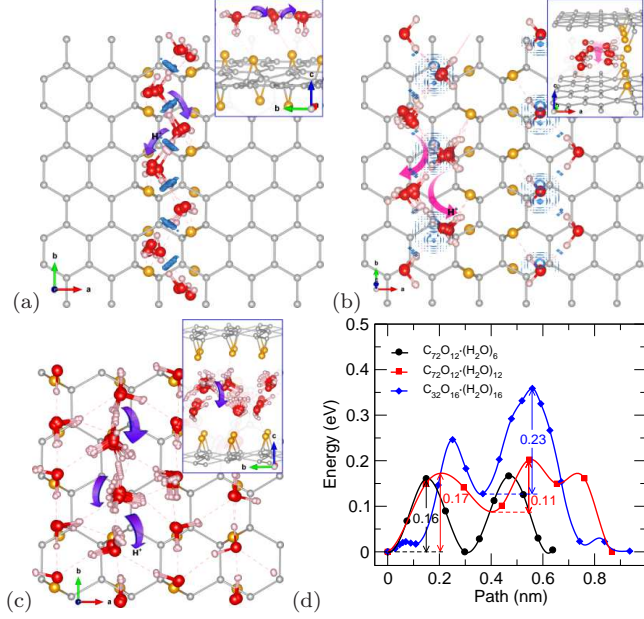


FIG. 6: Top view of migration paths for water-mediated proton transport in (a) monolayer  $C_{72}O_{12} \cdot 6(H_2O)$ , (b) bilayer  $C_{72}O_{12} \cdot 12(H_2O)$  and (c) bilayer  $C_{32}O_{16} \cdot 16(H_2O)$  rGO films. Insets show the perspective view, arrows indicate the proton migration, and blue isosurfaces in (a) and (b) represent the  $\Delta BVS$  at the value of 3. (d) Activation energies for these proton migrations.

tributed to hydrogen bonding interaction between the proton and adsorbed water molecules that are placed over epoxy groups, forming a hydrogen-bonded water channel. On the contrary, the activation energy in the case of bilayer  $C_{72}O_{12} \cdot 12(H_2O)$  model was determined to be higher as 0.63 eV. By inspecting the migration path, we found out that unlike the former case there is no hydrogen bond between the proton and intercalated water molecule in this model, in which water molecules are placed interlayer space away from the epoxy group row. Meanwhile, in the case of bilayer  $C_{32}O_{16} \cdot 16(H_2O)$  the proton migration was realized according to the mixed way of epoxy-water-mediated mechanism, although we enforced the epoxy-mediated migration. Here, the activation energies were estimated to be 0.48 eV for proton movement from water to epoxy group, which is occurred without hydrogen bonding interaction, and 0.37 eV along the epoxy-mediated path with the effect of hydrogen bond. These results indicate that the hydrogen bonding interaction between the proton and water molecule can enhance the in-plane proton transport.

In Figs. 6(a)–6(c), we show the migration paths for the water-mediated proton transport

in the monolayer  $C_{72}O_{12}\cdot 6(H_2O)$  and bilayer  $C_{72}O_{12}\cdot 12(H_2O)$  and  $C_{32}O_{16}\cdot 16(H_2O)$  models. As mentioned above, water molecules are connected with their neighbours by hydrogen bond, forming zigzag-type two-dimensional channel on the top of epoxy group (monolayer  $C_{72}O_{12}\cdot 6(H_2O)$  and bilayer  $C_{32}O_{16}\cdot 16(H_2O)$ ) or in the interlayer space ( $C_{72}O_{12}\cdot 12(H_2O)$ ). As clarified by  $\Delta BVS$  analysis, the inserted proton adhered to water molecule with the adsorption energies of  $-7.39$ ,  $-13.11$  and  $-12.76$  eV, forming hydronium ion ( $H_3O^+$ ), and then the nearest one of its three hydrogen ions moves to the neighbouring water molecule. Rotation of water molecules to some degree was observed during the proton migration. As shown in Fig. 6d, the corresponding activation energies were calculated to be 0.16, 0.17 and 0.23 eV in these hydrous rGO sheets, being much lower than along the epoxy-mediated paths and in the anhydrous GO sheet and comparable to the experimental value of 0.12 eV [1]. The similar values in the monolayer  $C_{72}O_{12}\cdot 6(H_2O)$  and the bilayer  $C_{72}O_{12}\cdot 12(H_2O)$  can be explained by the similar water-mediated paths, giving an evidence of indirect effect of epoxy groups, which play a role of holding the water molecules. Meanwhile, slightly higher value in the bilayer  $C_{32}O_{16}\cdot 16(H_2O)$  indicates that too many water molecules around the path may disturb the proton migration due to an attraction of the proton by another water molecule through hydrogen bonding interaction.

#### IV. CONCLUSIONS

In conclusion, we have studied the atomistic structures of water-adsorbed monolayer and water-intercalated bilayer rGO sheets, varying the oxidation degree and water content, and calculated the activation energies for the in-plane proton transports by applying the first-principles method. Our calculation has been shown to offer good agreement with experimental measures for interlayer distances of bilayer series as increasing the oxidation degree, shedding light on the hydrogen bond between water molecule and epoxy group. We suggest that in these hydrous rGO sheets the proton can migrate along two different mechanisms of epoxy- and water-mediated paths, and conclude that the water-mediated proton transport is actually occurred due to their much lower activation energy (0.16, 0.17 eV) compared to the epoxy-mediated transports and being close to the experimental value.

## Acknowledgments

This work is supported as part of the fundamental research project “Design of Innovative Functional Materials for Energy and Environmental Application” (no. 2016-20) funded by the State Committee of Science and Technology, DPR Korea. Computation was done on the HP Blade System C7000 (HP BL460c) that is owned by Faculty of Materials Science, Kim Il Sung University.

- 
- [1] K. Hatakeyama, M. R. Karim, C. Ogata, H. Tateishi, T. Taniguchi, M. Koinuma, S. Hayami, and Y. Matsumoto, *Optimization of proton conductivity in graphene oxide by filling sulfate ions*, Chem. Commun. **50**, 14527 (2014).
  - [2] K. Hatakeyama, H. Tateishi, T. Taniguchi, M. Koinuma, T. Kida, S. Hayami, H. Yokoi, and Y. Matsumoto, *Tunable graphene oxide proton/electron mixed conductor that functions at room temperature*, Chem. Mater. **26**, 5598 (2014).
  - [3] K. Hatakeyama, M. S. Islam, K. Michio, C. Ogata, T. Taniguchi, A. Funatsu, T. Kida, S. Hayami, and Y. Matsumoto, *Super proton/electron mixed conduction in graphene oxide hybrids by intercalating sulfate ions*, J. Mater. Chem. A **3**, 20892 (2015).
  - [4] K. Hatakeyama, M. R. Karim, C. Ogata, H. Tateishi, A. Funatsu, T. Taniguchi, M. Koinuma, S. Hayami, and Y. Matsumoto, *Proton conductivities of graphene oxide nanosheets: Single, multilayer, and modified nanosheets*, Angew. Chem. Int. Ed. **53**, 6997 (2014).
  - [5] M. R. Karim, K. Hatakeyama, T. Matsui, H. Takehira, T. Taniguchi, M. Koinuma, Y. Matsumoto, T. Akutagawa, T. Nakamura, S. Noro, et al., *Graphene oxide nanosheet with high proton conductivity*, J. Am. Chem. Soc. **135**, 8097 (2013).
  - [6] K. Wakata, M. S. Islam, M. R. Karim, K. Hatakeyama, N. N. Rabin, R. Ohtani, M. Nakamura, M. Koinuma, and S. Hayami, *Role of hydrophilic groups in acid intercalated graphene oxide as a superionic conductor*, RSC Advances **7**, 21901 (2017).
  - [7] M. Koinuma, C. Ogata, Y. Kamei, K. Hatakeyama, H. Tateishi, Y. Watanabe, T. Taniguchi, K. Gezuhara, S. Hayami, A. Funatsu, et al., *Photochemical engineering of graphene oxide nanosheets*, J. Phys. Chem. C **116**, 19822 (2012).
  - [8] S. Hu, M. Lozada-Hidalgo, F. C. Wang, A. Mishchenko, F. Schedin, R. R. Nair, E. W. Hill,

- D. W. Boukhvalov, M. I. Katsnelson, R. A. W. Dryfe, et al., *Proton transport through one-atom-thick crystals*, Nature **516**, 227 (2014).
- [9] M. I. Walker, P. Braeuninger-Weimer, R. S. Weatherup, S. Hofmann, and U. F. Keyser, *Measuring the proton selectivity of graphene membranes*, Appl. Phys. Lett. **107**, 213104 (2015).
- [10] K. Goh, H. E. Karahan, L. Wei, T.-H. Bae, A. G. Fane, R. Wang, and Y. Chen, *Carbon nanomaterials for advancing separation membranes: A strategic perspective*, Carbon **109**, 694 (2016).
- [11] L. Shi, A. Xu, G. Chen, and T. Zhao, *Theoretical Understanding of Mechanisms of Proton Exchange Membranes Made of 2D Crystals with Ultrahigh Selectivity*, J. Phys. Chem. Lett. **8**, 4354 (2017).
- [12] H. W. Kim, H. W. Yoon, S. M. Yoon, B. M. Yoo, B. K. Ahn, Y. H. Cho, H. J. Shin, H. Yang, U. Paik, S. Kwon, et al., *Selective gas transport through few-layered graphene and graphene oxide membranes*, Science **342**, 91 (2013).
- [13] H. Li, Z. N. Song, X. J. Zhang, Y. Huang, S. G. Li, Y. T. Mao, H. J. Ploehn, Y. Bao, and M. Yu, *Ultrathin, molecular-sieving graphene oxide membranes for selective hydrogen separation*, Science **342**, 95 (2013).
- [14] R. K. Joshi, P. Carbone, F. C. Wang, V. G. Kravets, Y. Su, I. V. Grigorieva, H. A. Wu, A. K. Geim, and R. R. Nair, *Precise and ultrafast molecular sieving through graphene oxide membranes*, Science **343**, 752 (2014).
- [15] L. Tsetseris and S. T. Pantelides, *Graphene: an impermeable or selectively permeable membrane for atomic species?*, Carbon **67**, 58 (2014).
- [16] V. Berry, *Impermeability of graphene and its applications*, Carbon **62**, 1 (2013).
- [17] M. Miao, M. B. Nardelli, Q. Wang, and Y. Liu, *First principles study of the permeability of graphene to hydrogen atoms*, Phys. Chem. Chem. Phys. **15**, 16132 (2013).
- [18] W. L. Wang and E. Kaxiras, *Graphene hydrate: theoretical prediction of a new insulating form of graphene*, New J. Phys. **12**, 125012 (2010).
- [19] Y. Zhao and T. Gennett, *Water-mediated cooperative migration of chemisorbed hydrogen on graphene*, Phys. Rev. Lett. **112**, 076101 (2014).
- [20] Z. Šljivančanin, A. S. Milošević, Z. S. Popović, and F. R. Vukajlović, *Binding of atomic oxygen on graphene from small epoxy clusters to a fully oxidized surface*, Carbon **54**, 482 (2013).
- [21] L. Wang, Y. Y. Sun, K. Lee, D. West, Z. F. Chen, J. J. Zhao, and S. B. Zhang, *Stability of*

- graphene oxide phases from first-principles calculations*, Phys. Rev. B **82**, 161406 (2010).
- [22] M. Topsakal and S. Ciraci, *Domain formation on oxidized graphene*, Phys. Rev. B **86**, 205402 (2012).
- [23] A. M. Dimiev, L. B. Alemany, and J. M. Tour, *Graphene Oxide. Origin of Acidity, Its Instability in Water, and a New Dynamic Structural Model*, ACS Nano **7**, 576 (2013).
- [24] K. Raidongia and J. Huang, J. Am. Chem. Soc. **134**, 16528 (2012).
- [25] L. Zhao, Y. Li, H. Zhang, W. Wu, J. Liu, and J. Wang, *Constructing proton-conductive highways within an ionomer membrane by embedding sulfonated polymer brush modified graphene oxide*, J. Power Sources **286**, 445 (2015).
- [26] C.-Y. Tseng, Y.-S. Ye, M.-Y. Cheng, K.-Y. Kao, W.-C. Shen, J. Rick, J.-C. Chen, and B.-J. Hwang, *Sulfonated polyimide proton exchange membranes with graphene oxide show improved proton conductivity, methanol crossover impedance, and mechanical properties*, Adv. Energy Mater. **1**, 1220 (2011).
- [27] I. Nicotera, C. Simari, L. Coppola, P. Zygouri, D. Gournis, S. Brutti, F. D. Minuto, A. S. Aricó, D. Sebastian, and V. Baglio, *Sulfonated graphene oxide platelets in nafion nanocomposite membrane: Advantages for application in direct methanol fuel cells*, J. Phys. Chem. C **118**, 24357 (2014).
- [28] J. Klimeš, D. R. Bowler, and A. Michaelides, Phys. Rev. B **83**, 195131 (2011).
- [29] P. Giannozzi, S. Baroni, N. Bonini, M. Calandra and R. Car, et al., *QUANTUM ESPRESSO: a modular and open-source software project for quantum simulations of materials*, J. Phys.:Condens. Matter **21**, 395502 (2009).
- [30] J. P. Perdew, K. Burke, and M. Ernzerhof, *Generalized gradient approximation made simple*, Phys. Rev. Lett. **77**, 3865 (1996).
- [31] I. D. Brown and D. Altermatt, *Bond-valence parameters obtained from a systematic analysis of the inorganic crystal structure database*, Acta Crystallogr. B. Struct. Sci. **41**, 244 (1985).
- [32] M. O’Keeffe and N. E. Brese, *Atom sizes and bond lengths in molecules and crystals*, J. Am. Chem. Soc. **113**, 3226 (1991).
- [33] G. S. Rohrer, *Structure and Bonding in Crystalline Materials* (Cambridge University Press, 2004).
- [34] G. Henkelman, B. P. Uberuaga, and H. Jónsson, *A climbing image nudged elastic band method for finding saddle points and minimum energy paths*, J. Chem. Phys. **113**, 9901 (2000).

- [35] A. Paneri and S. Moghaddam, *Impact of synthesis conditions on physicochemical and transport characteristics of graphene oxide laminates*, Carbon **86**, 245 (2015).
- [36] A. Paneri, Y. Heo, G. Ehlert, A. Cottrill, H. Sodano, P. Pintauro, and S. Moghaddam, *Proton selective ionic graphene-based membrane for high concentration direct methanol fuel cells*, J. Memb. Sci. **467**, 217 (2014).
- [37] J.-A. Yan, L. Xian, and M. Y. Chou, *Structural and electronic properties of oxidized graphene*, Phys. Rev. Lett. **103**, 086802 (2009).
- [38] See supplementary material at URL for more details regarding calculations and analysis.
- [39] We used C.pbe-van\_ak.UPF, O.pbe-van\_ak.UPF, and H.pbe-van\_ak.UPF, which are provided in the package.